ADVANCED ENERGY MATERIALS
www.advenergymat.de

Photo De-Mixing in Dion-Jacobson 2D Mixed Halide Perovskites

Ya-Ru Wang, Alessandro Senocrate, Marko Mladenović, Algirdas Dučinskas, Gee Yeong Kim, Ursula Rothlisberger, Jovana V. Milić, Davide Moia, Michael Grätzel, and Joachim Maier**

2D halide perovskites feature a versatile structure, which not only enables the fine-tuning of their optoelectronic properties but also makes them appealing as model systems to investigate the fundamental properties of hybrid perovskites. In this study, the authors analyze the changes in the optical absorption of 2D Dion-Jacobson mixed halide perovskite thin films (encapsulated) based on (PDMA)Pb($I_{0.5}Br_{0.5}$)$_4$ (PDMA: 1,4-phenylenedimethanammonium spacer) exposed to a constant illumination. It is demonstrated that these 2D mixed-halide perovskites undergo photo-induced phase segregation, where the pristine mixed-phase de-mixes into iodide-rich and bromide-rich phases (photo de-mixing). The de-mixed state is largely maintained in the dark at room temperature for several months, while at higher temperatures it shows complete reversibility to the mixed-phase in terms of optical and structural properties (dark re-mixing). The authors further investigate temperature-dependent absorption measurements under light to extract the photo de-mixed compositions and to map the photo-miscibility-gap. This work thereby reveals that reversible photo de-mixing occurs in Dion-Jacobson 2D hybrid perovskites and provides strategies to address the role of light in the thermodynamic properties of these materials.

1. Introduction

Organic–inorganic hybrid halide perovskites show intriguing application potential for various optoelectronic devices, including solar cells,[1] light-emitting diodes,[2] field-effect transistors,[3] and photodetectors.[4] 3D perovskites with the general formula ABX_3 (A cation placed in the cavities of corner-sharing BX_6 octahedra network) are prime candidates as light harvesters in solar cells.[5] 2D hybrid perovskites add additional degrees of freedom to modulate the electronic and optical properties of halide perovskites with large organic cations (spacers) separating layers of corner-sharing metal halide octahedra.[6] Depending on the relative orientation of the inorganic slabs and the spacer, these systems can be classified into Ruddlesden–Popper (RP) ($A'_2A_{n-1}B_nX_{3n+1}$, mostly A′ monovalent spacer separating the inorganic slabs with half-a-unit-cell relative offset)[7] and Dion–Jacobson (DJ) ($A''A_{n-1}B_nX_{3n+1}$, mostly A″ divalent spacer separating well-aligned inorganic slabs) phases.[8] Here, n represents the number of the metal halide planes between spacer planes.[9]

Apart from the nature of the organic cations, halide substitution or mixing provide an effective way to vary the material properties of both 2D and 3D halide perovskites.[10–12] However, 3D mixed halide perovskites (e.g., $MAPb(I_{0.5}Br_{0.5})_3$) have

Y.-R. Wang, A. Senocrate, A. Dučinskas, G. Y. Kim, D. Moia, M. Grätzel, J. Maier
Max Planck Institute for Solid State Research
70569 Stuttgart, Germany
E-mail: d.moia@fkf.mpg.de; office-maier@fkf.mpg.de

The ORCID identification number(s) for the author(s) of this article can be found under https://doi.org/10.1002/aenm.202200768.

[+]Present address: Integrated Systems Laboratory, ETH Zürich, Zurich 8092, Switzerland

[++]Present address: Adolphe Merkle Institute, University of Fribourg, Fribourg 1700, Switzerland

M. Mladenović,[+] U. Rothlisberger
Laboratory of Computational Chemistry and Biochemistry
Institute of Chemical Sciences and Engineering
École Polytechnique Fédérale de Lausanne (EPFL)
Lausanne CH-1015, Switzerland

A. Dučinskas, J. V. Milić,[++] M. Grätzel
Laboratory of Photonics and Interfaces
Ecole polytechnique Fédérale de Lausanne (EPFL)
Lausanne CH-1015, Switzerland

DOI: 10.1002/aenm.202200768

been shown to undergo segregation under illumination into Br-rich and I-rich compositions (photo de-mixing). Such segregation process appears to be largely reversible as in the dark the de-mixed phases re-mix to form the original phase (dark re-mixing).[13,14] Various studies investigated photo de-mixing in mixed halide perovskites, some of them describing the materials' miscibility gap based on thermodynamic and kinetic arguments.[15] While the possible existence of a miscibility gap in the dark has been discussed,[10,16] the fact that this is a reversible process points towards the generally accepted interpretation that illumination changes the thermodynamics of these mixtures. Factors such as polaron formation and strain effects,[17] bandgap reduction due to iodide rich phase formation,[18,19] influence from local electric fields,[20] halide oxidation[21] were proposed to explain the thermodynamic origin of photo de-mixing. In our recent work, we have invoked selective self-trapping in iodide-based and bromide-based perovskites as a possible factor contributing to the driving force for the process.[22] The large polarizability associated with the iodide-rich environment favors self-trapping of photo-generated holes related with iodine interstitial formation. Hole accumulation achieved by contacting mixed halide perovskites with electron transport layers[20,23] and through electrochemical anodic bias[24] also provide direct experimental evidence for the important role of the hole concentration on the photo de-mixing behavior in 3D mixed halide perovskites. Reports on the reversible Pb^{2+}/Pb^0 and I^-/I^{3-} redox chemistry under light also gave important insights into the possible trapping mechanisms.[25]

Elucidating the origin of photo de-mixing and its relation to ion transport and defect chemistry of mixed halide perovskites is of substantial conceptual importance, as it would provide guidelines for suppressing photo-induced phase instability, optimizing halide alloying, and opening up opportunities for new optoelectronic devices.[26] Evidence for suppressed ion transport in 2D halide perovskites compared with classic 3D hybrid perovskites,[27,28] as well as enhancement of ion transport under light in 2D systems have been suggested.[29] Recently, photo de-mixing in 2D RP mixed halide perovskites was reported, also emphasizing the role of the spacer and of the *n* value in dictating the occurrence and kinetics of the photo-induced phase segregation respectively.[30,31] A number of remaining questions related to photo de-mixing in 2D mixed halide perovskites require clarification, including the degree of reversibility of this process, the evaluation of the compositions of the de-mixed phases, and the effect of bifunctional organic spacers relevant to DJ systems. More in general, the understanding of the phase behavior of 2D halide perovskites would shed light on fundamental questions related to the role of confinement in the determination of their ionic properties. These aspects have not been addressed in detail to date. The improved stability of 2D perovskites[28] compared to their 3D counterparts also makes them suitable model systems for investigating photo de-mixing, given the challenge to decouple photo de-mixing from light-induced degradation.[32]

Here, we report on photo de-mixing and dark re-mixing for 2D Dion-Jacobson thin films $(PDMA)Pb(I_{0.5}Br_{0.5})_4$ based on 1,4-phenylenedimethanammonium ($PDMA^{2+}$) spacer. By monitoring the in situ evolution of optical absorption and X-ray diffraction (XRD), we demonstrate that encapsulated 2D mixed-halide perovskites undergo de-mixing under illumination with complete re-mixing in the dark both optically and structurally. Finally, we developed and compared experimental methods

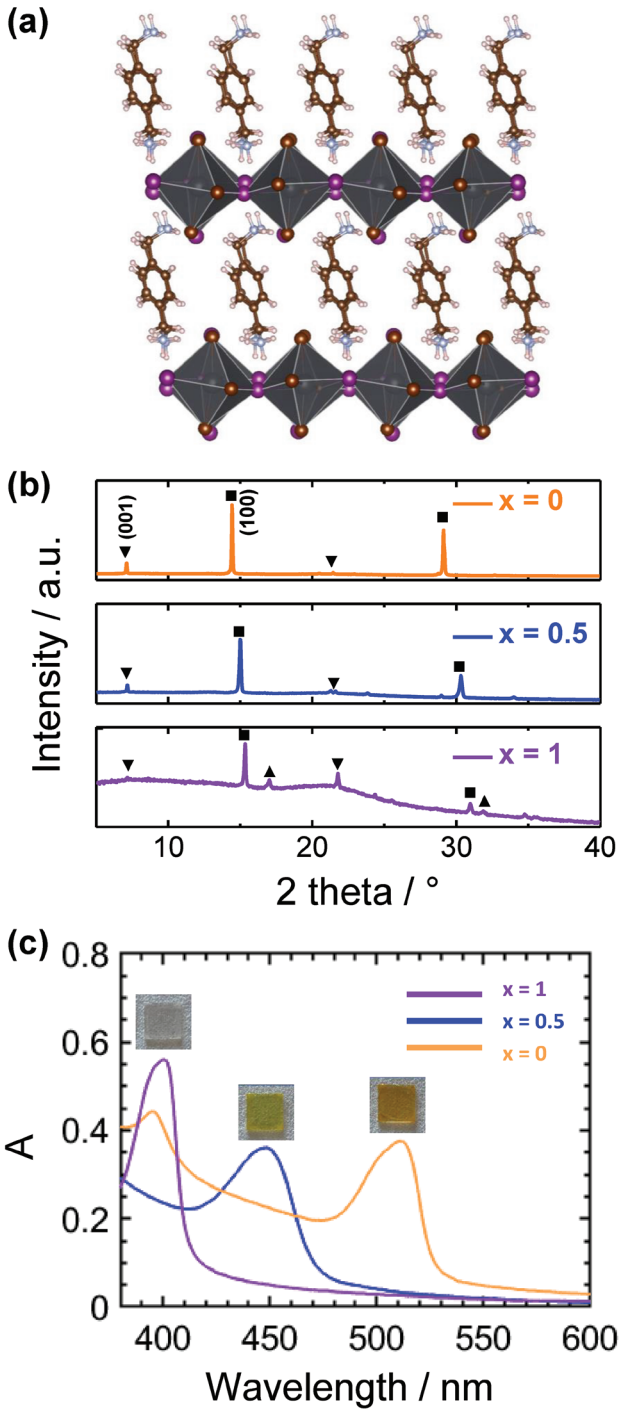

Figure 1. a) Schematic representation of the $(PDMA)Pb(I_{1-x}Br_x)_4$ ($n = 1$) layered structure; b) XRD patterns and c) UV–Vis spectra of 2D layered perovskite thin films on quartz substrates: $(PDMA)PbI_4$ (yellow line), $(PDMA)Pb(I_{0.5}Br_{0.5})_4$ (blue line), $(PDMA)PbBr_4$ (purple line). Diffraction peaks in (b) are labeled with ▼, ▲, and ■ representing (00l), (0k0), and (h00) Bragg planes, respectively. Photographs of relevant thin film samples with corresponding compositions are included in the inset of (c).

that can be used to investigate the phase behavior of materials that undergo photo de-mixing. Based on the analysis of the temperature-dependent absorption spectra of films under illumination, we provide information on the photo-induced miscibility gap for 2D Dion-Jacobson mixed halide perovskites.

2. Results and Discussion

2D Dion-Jacobson halide perovskite thin films based on $(PDMA)Pb(I_{1-x}Br_x)_4$ composition (**Figure 1**a) with Br content $x = 0$ ($(PDMA)PbI_4$), $x = 0.5$ ($(PDMA)Pb(I_{0.5}Br_{0.5})_4$), and $x = 1$ ($(PDMA)PbBr_4$) were fabricated following the procedure described in Section S1, Supporting Information. All films were measured in Ar atmosphere encapsulated with poly(methyl methacrylate) (PMMA) unless otherwise stated to minimize photo-induced degradation during the characterization of photo de-mixing.

Figure 1b shows the XRD patterns of these films. The diffraction peaks at low angles can be ascribed to reflections from the (001) crystal planes ($2\theta = 7.11°$, 7.16°, 7.19° for $x = 0$, 0.5, and 1, respectively) and correspond to the expected Pb—Pb interlayer distance, indicating the successful preparation of the layered structure for these thin films.[33] The increase of the bromide content results in a decrease in such distance (12.43, 12.34, and 12.30 Å for $x = 0$, 0.5, and 1, respectively), due to the smaller radius of the bromide ion compared with the iodide ion. Calculated diffraction data using density functional theory of optimized structural models allow us to identify the observed peaks, corresponding to different orientations (as indicated in Figure 1b). For the mixed halide composition $x = 0.5$, we explored several different possible arrangements of the iodide and bromide ions in the structure (mixtures 1–4) and calculated their structural and electronic properties (see Section S2 and Figure S4, Supporting Information). The results indicate that the intermediate composition ($x = 0.5$) with the halides in mixed configurations shows a larger free energy than the end members ($x = 0$, $x = 1$), with the exception of the inhomogeneous mixture (mixture 4), for which we obtained a slightly lower free energy compared to the end members. This suggests that lack of miscibility for intermediate compositions would be expected, similarly to the conclusion of early report on 3D mixed halide systems.[15] We have further analyzed thin films by UV–Vis absorption spectroscopy. The data highlights a pronounced excitonic absorption peak for each of the films (Figure 1c), which can be attributed to the optical transitions in the 2D quantum wells.[34] By increasing the Br content, the wavelength associated with the excitonic peak decreases (512, 450, 401 nm), in accordance with the expected changes in the resulting optical properties of layered perovskite materials.[11,35] We have also demonstrated the successful fabrication of thin films with other intermediate compositions (see Figure S5, Supporting Information).

Having evidenced the formation of 2D structures in thin films, we monitored the in situ evolution of their optical response changes under illumination using UV–Vis. This technique enables in situ non-destructive evaluation of optical and structural properties[36] and is commonly used to probe photo de-mixing in mixed halide perovskites.[37]

The exposure to light induced no significant change in the optical absorption spectrum of the $x = 0$ (iodide) and minor changes for the $x = 1$ (bromide) 2D perovskite thin films (Figure S6, Supporting Information). Such changes are not related to de-mixing (only one halide involved) or to temperature variations and have been also observed for pure I- and pure Br-RP films under light.[38] On the other hand, we observed a pronounced change in the absorbance for a thin film of the 50% iodide 50% bromide composition under illumination. In the following, we refer to the initial homogeneous composition of the film before exposure to light as $x_{initial}$ (in this case $x_{initial} = 0.5$). The spectral evolution indicates a gradual phase transformation from the pristine phase $(PDMA)Pb(I_{0.5}Br_{0.5})_4$ to Br-rich and I-rich phases (**Figure 2**a; the curves' color gradient from black to red refers to early to long time scale of illumination). Strikingly, during photo de-mixing, the absorbance of the sample remains approximately invariant for the two wavelengths $\lambda_1 = 432$ nm and $\lambda_2 = 463$ nm. The presence of these isosbestic points suggests that direct transformation from the pristine $x_{initial} = 0.5$ composition to a second state comprising I-rich and Br-rich phases may occur. The change in absorbance ΔA (Figure 2c), obtained by subtracting the initial absorbance spectrum before illumination from each subsequent spectrum, clearly shows the formation of I-rich and Br-rich phases and bleaching of the feature assigned to $(PDMA)Pb(I_{0.5}Br_{0.5})_4$. The shape of ΔA remains approximately similar as a function of illumination time, suggesting that the phases that form at early time scales are already close in composition to the final quasi-equilibrium phases.

After photo de-mixing, illumination was removed and the sample was left in the dark. As a result, the de-mixed phases underwent re-mixing (Figure 2b). Only a small difference between the pristine absorption spectrum and the one after re-mixing for ≈330 h in the dark (blue and red dashed lines in Figure 2b) was observed, indicating almost full reversibility for the sample's optical properties. The kinetics of the change in absorbance ΔA during the experiment (displayed in Figure 2e,f) emphasizes the difference in time scale between the de-mixing (≈10 h) and re-mixing (≈330 h) processes.

To further clarify the optical and structural reversibility of photo de-mixing in these 2D mixtures, we performed UV–vis and XRD measurements on a $(PDMA)Pb(I_{0.5}Br_{0.5})_4$ thin film sample in its pristine state and after 4 consecutive treatments. These include a photo de-mixing and 3 dark re-mixing steps, as shown in **Figure 3**a. The UV–Vis and XRD data were collected at room temperature and are shown in Figure 3b,c. After illumination at 80 °C for 20 h (step(1)), we observe the emergence of both longer (I-rich) and shorter (Br-rich) wavelength optical absorption features, consistently with Figure 2, accompanied by a decrease in the diffraction intensity and broadening of some XRD peaks. The structural change seems to affect predominantly peaks that correspond to the (h00) orientation (Figure S10, Supporting Information). Regarding the dark re-mixing experiment, only limited changes are detected when storing the thin film in argon in the dark at room temperature for 6 months (step(2)). On the other hand, after leaving the thin film at 80 °C for 30 days (step(3) and step(4)), the de-mixed phases re-mixed reaching a state close to the pristine phase, from both absorption and structural analysis.

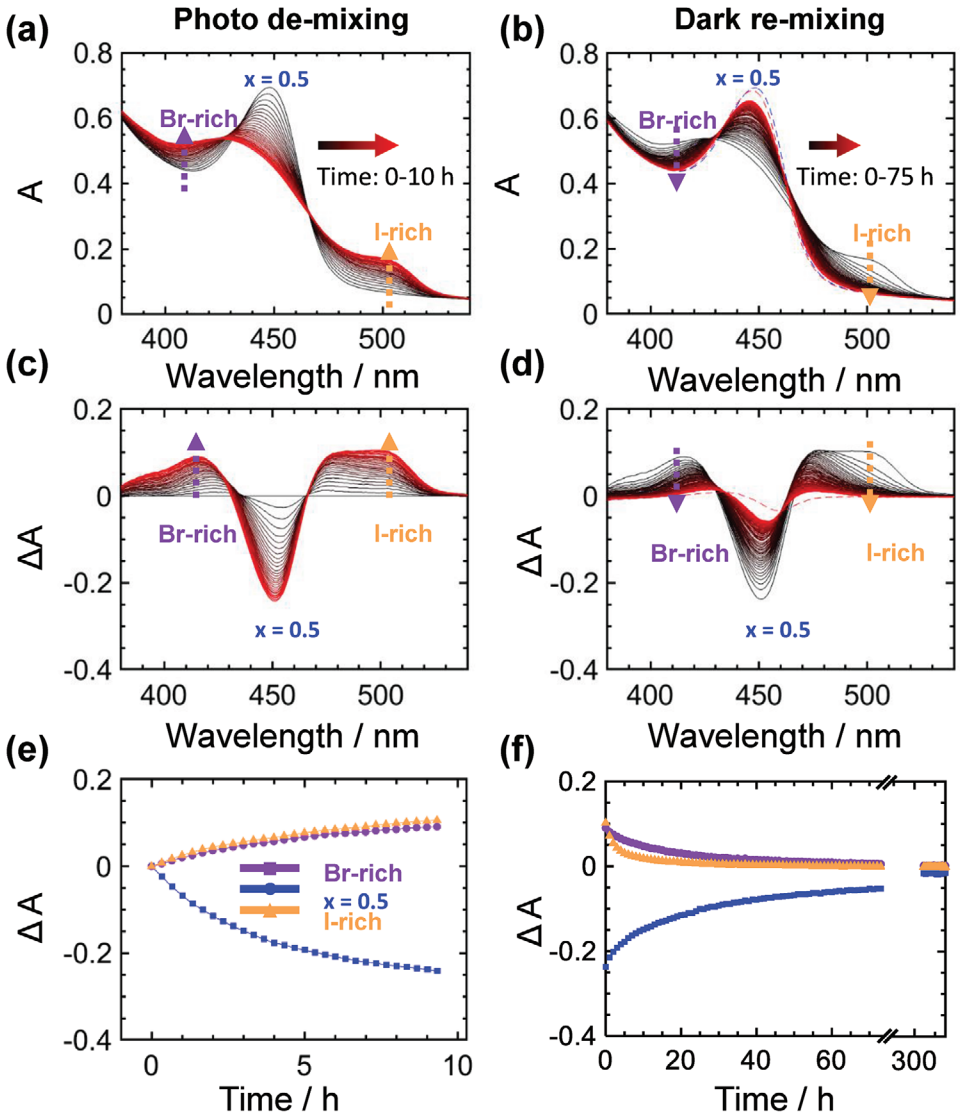

Figure 2. UV–Vis spectra evolution of (PDMA)$Pb(I_{0.5}Br_{0.5})_4$ thin films (with PMMA encapsulation and in Ar atmosphere to exclude possible degradation) a) under light (1.5 mW cm^{-2}) at 80 °C for ≈10 h with 20 min interval and b) in the dark at 80 °C for ≈75 h with 1 h time interval between measurements. For the case under light, within each interval, spectra are collected by switching off the bias light for 300 s (see Section S1 and Figure S1, Supporting Information). The gradient from black to red in (a–d) denotes the time sequence. In (b), the blue dashed line represents the absorption spectra of the sample before illumination (also shown in (a) for Time = 0 h), while the red dashed line corresponds to the absorbance after photo de-mixing and 330 h of re-mixing in the dark. c,d) Change in absorbance obtained by subtracting the reference spectrum of the pristine sample from each absorbance spectrum shown in (a,b), respectively. e,f) Kinetics of the photo de-mixing and dark re-mixing processes highlighting the change in absorbance at wavelengths associated to (PDMA)$Pb(I_{0.5}Br_{0.5})_4$ (450 nm, blue), Br-rich (414 nm, purple) and I-rich (501 nm, yellow) phases.

To investigate the dependence of the observed reversibility in the optical and structural properties on the de-mixing temperature, we performed the same experiment illustrated in Figure 3a, using different temperatures for step(1). We show the complete datasets in Section S5 and Figures S7–S12, Supporting Information. We find that the decrease in intensity and broadening of some diffraction peaks are more pronounced for higher photo de-mixing temperatures, consistent with a larger fraction of the film undergoing phase separation (see peak intensity and FWHM of the (h00) orientation in Figure 3d). As for the re-mixing in the dark, once again we observe limited changes in properties after step(2), while complete reversibility to the mixed state is gradually reached after step(3) and (4). This experiment highlights the long-term reversible behavior associated with photo de-mixing and dark re-mixing in these 2D mixed-halide perovskite thin films. In particular, i) we demonstrate a large degree of reversibility in terms of optical properties for samples that were de-mixed at different temperatures and for over 20 h; ii) for some of the samples the reversibility is complete also concerning their structural properties; iii) the data show the possibility to kinetically trap the photo de-mixed state by storing the sample in the dark at room temperature.

In order to investigate more in detail the properties of the miscibility gap for these compounds when exposed to light,

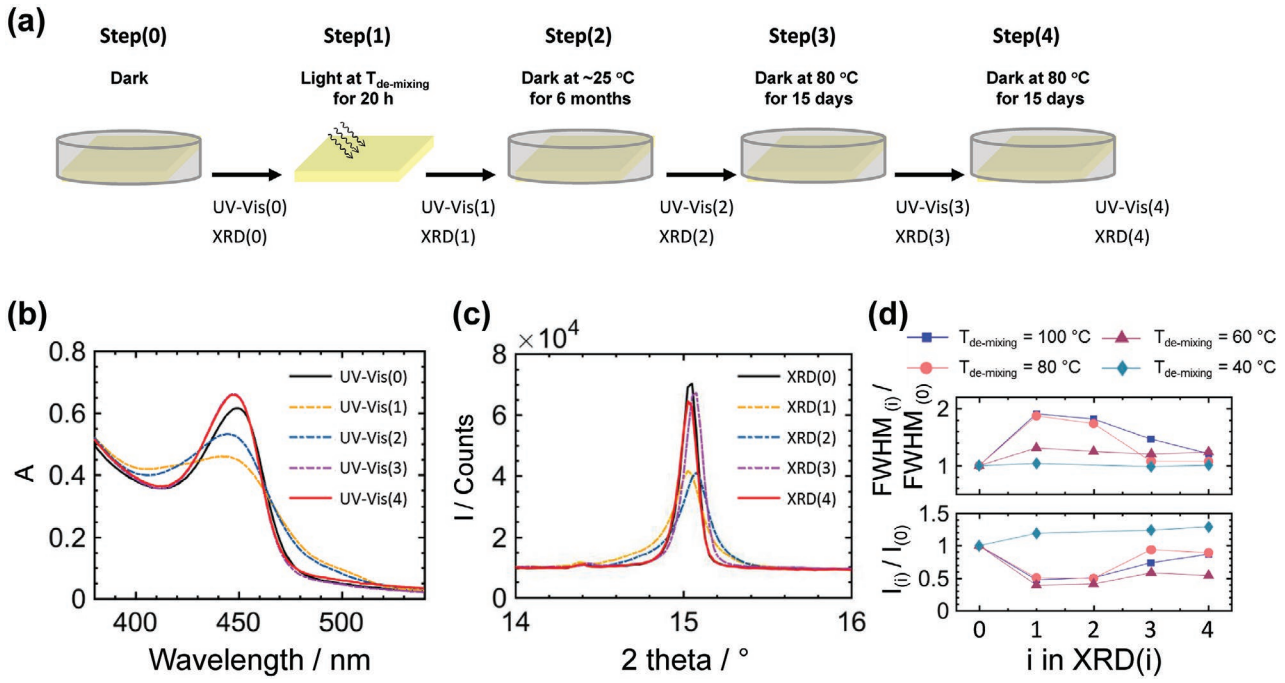

Figure 3. a) Schematics showing the experimental procedure performed on (PDMA)Pb$(I_{0.5}Br_{0.5})_4$ thin films (with PMMA encapsulation). All steps are performed in argon atmosphere. Step(0): pristine film in the dark; step(1): illuminating the thin film using cold white LED with 1.5 mW cm^{-2} for 20 h at a temperature of $T_{de\text{-}mixing}$; step(2): thin-film stored in the dark at room temperature for 6 months; step(3): thin-film left at 80 °C for 15 days in the dark; step(4): thin-film left at 80 °C for another 15 days in the dark. Both XRD and UV–Vis measurements are conducted at room temperature after each step. b) UV–Vis and c) XRD performed after each treatment step shown in (a) on thin films $T_{de\text{-}mixing}$ = 80 °C. d) Changes in relative FWHM and intensity for XRD peak 2θ = 13–17° after each step, for thin films that are de-mixed at different temperatures (see also data in Figures S7–S12, Supporting Information).

which we will refer to as photo-miscibility-gap, we carried out temperature-dependent UV–Vis absorption measurements of a thin film with $x_{initial}$ = 0.5. For this experiment, we used the same illumination conditions as described in Figures 2 and 3. After performing photo de-mixing of the sample at 100 °C for 20 h, the temperature was gradually decreased to 40 °C, with the illumination intensity being kept constant. As shown in **Figure 4**, while no significant change was observed for the shape of the feature associated to the Br-rich phase, the absorption signal detected for the I-rich phase showed a significant redshift with decreasing temperature. The reversibility of the process was inspected by performing a second temperature scan back to high temperature under the same conditions (Figure 4b,d). Strikingly, the absorption features of the I-rich phase shifted back to the same wavelength region as originally observed for the same temperature, suggesting a reversible behavior. To provide a quantitative evaluation of the temperature dependence of the de-mixed compositions under light, we extracted characteristic absorption wavelengths associated with the Br-rich and I-rich domains. The characteristic absorption wavelengths of Br-rich phases were determined based on the peak position of the ΔA spectra at short wavelengths. We then converted these values into compositions (x_{Br}) by using a calibration dataset obtained from calculated ΔA spectra based on the absorption of films with different compositions at different temperatures. This method allows us to account for the overlapping absorption features from different phases at short wavelengths and possible temperature effects. For the I-rich phase, we considered the position of the (negative) peak in slope of the experimental ΔA, which we then converted into composition (x_I) based on the calibration data obtained from the calculated ΔA spectra described above. For detailed information on the method used to extract the composition of the de-mixed phases, see Section S6, Supporting Information (Figures S14–S19, Supporting Information).

The data (summarized in Figure 4e) show that, by decreasing the temperature, the gap for the de-mixed compositions widens. The photo de-mixed composition for the I-rich domain approaches the value corresponding to the end member composition (x = 0). The feature associated to the Br-rich domain undergoes much more limited changes over the probed temperature range. This indicates that the degree of de-mixing, and therefore the range of immiscible compositions, increases in width with decreasing temperature, which is consistent with the decrease in the molar entropy of mixing contribution to the free energy when decreasing temperature. As discussed above, the analysis of the upward temperature scan (shown by △) displays an analogous trend. The critical temperature of this photo-miscibility gap, above which the entropic contribution would be large enough to prevent de-mixing, is an important parameter. We limited our investigation of long time-scale photo de-mixing to temperatures $T \leq 100$ °C, to avoid possible changes in the film's properties (annealing temperature of 150 °C was used during film preparation). However, we note that UV-Vis measurements performed on a sample with $x_{initial}$ = 0.5 under light at 150 °C showed the appearance of absorption features

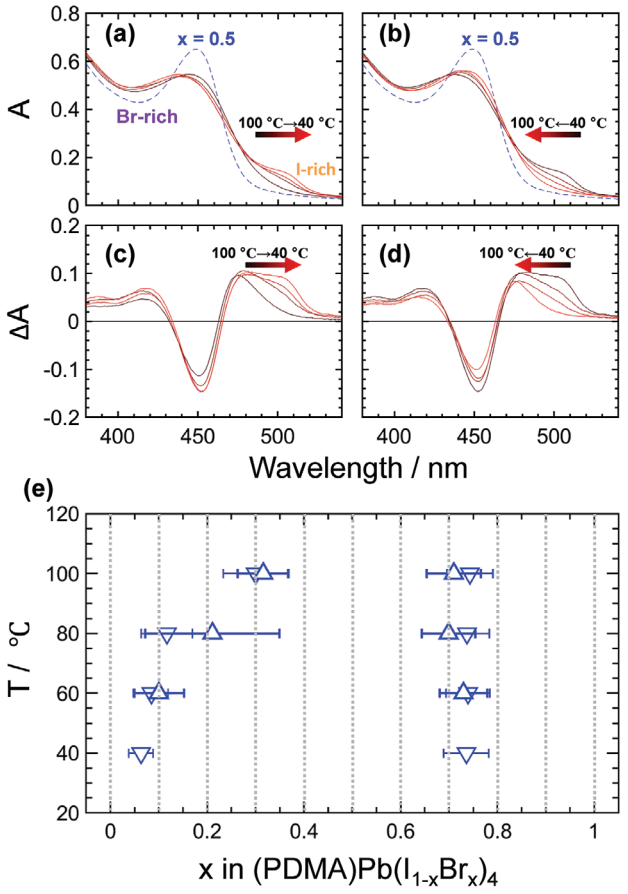

Figure 4. Temperature-dependent UV–Vis measurements performed on a (PDMA)$Pb(I_{0.5}Br_{0.5})_4$ thin film (with PMMA encapsulation) under light (1.5 mW cm^{-2}) at temperature varying as follows: a) 100 °C → 80 °C → 60 °C → 40 °C, b) 40 °C → 60 °C → 80 °C → 100 °C (displayed spectra are recorded after 20 h at each temperature). The gradient color from black to red denotes the sequence of the temperature steps. The dashed blue lines indicate the absorption spectrum of the pristine (PDMA)$Pb(I_{0.5}Br_{0.5})_4$ phase ($x_{initial}$ = 0.5) at 100 °C. c–d) Change in absorbance ΔA spectra (obtained by subtracting from each absorption spectrum the spectrum of the pristine sample). e) Photo-miscibility-gap extracted from temperature-dependent UV–Vis measurements shown in (a–d); Downward-pointing (▽) and upward-pointing (△) triangles denote data collected during a downward and upward temperature scan respectively (for details on the method to evaluate the photo-miscibility gap, see text and Section S5, Supporting Information).

associated with Br-rich and I-rich phases at early time scales (Figure S24, Supporting Information). We cannot easily extract photo de-mixed compositions for such phases due to the disappearance of the I-rich feature at long time scales. Nevertheless, this experiment suggests a critical temperature higher than 150 °C and provides a lower bound estimate of 0.07 eV for the interaction parameter Ω ($\Omega = T_c/2R$, where R is the gas constant).[39]

Regarding the temperature-dependent UV–Vis experiment shown in Figure 4, XRD measurements were also taken after each temperature step to evaluate the influence of light and temperature on the film's structural properties. Compared to the XRD measurement performed on the pristine sample, we observed a decrease in peak intensity and broadening of peak width upon illumination during the first temperature step, consistent with the data in Figure 3. However, negligible changes in the XRD pattern were detected for all of the following temperature steps (Figure S25, Supporting Information). This result suggests that, while the structural properties of the film do change upon exposure to light, a new stable structure is reached and maintained throughout the experiment.

To further investigate the role of these structural changes on the photo-miscibility gap, we analyzed the optical data (Figures S27 and S28, Supporting Information) collected during the experiment described in Figure 3, where different pristine samples were used for each of the photo de-mixing temperatures. We find that: i) the Br-rich and I-rich compositions extracted as a function of illumination time during these experiments (Figures S22 and S23, Supporting Information) show negligible changes in the time range of 10–20 h, suggesting that stable compositions are reached for all de-mixed temperatures; ii) The obtained de-mixed compositions for

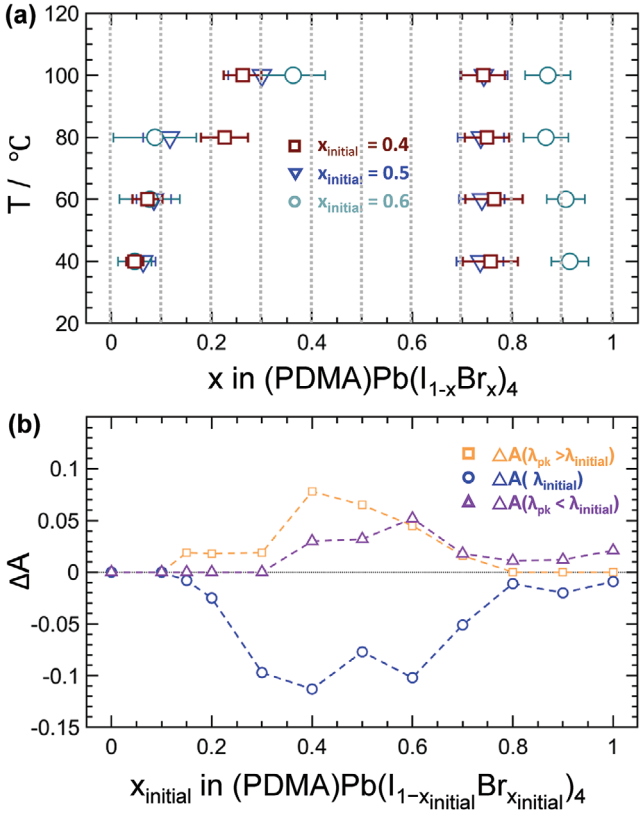

Figure 5. Photo de-mixing study on thin films of (PDMA)$Pb(I_{1-x}Br_x)_4$ with different initial composition performed under illumination (1.5 mW cm^{-2}). a) Photo-miscibility-gap extracted from temperature-dependent UV-Vis. Films with $x_{initial}$ = 0.4 (brown), $x_{initial}$ = 0.5 (blue), and $x_{initial}$ = 0.6 (cyan) are considered. The data correspond to measurements of the films taken after 20 h at each temperature under continuous illumination. b) Changes in absorbance ΔA measured at 100 °C and after 2 h of illumination plotted as function of the films' initial composition. The dataset indicated by the blue circles displays the bleach in the absorption at $\lambda_{initial}$ (peak wavelength of the pristine film). The yellow squares and the purple triangles indicate the peak values of ΔA features that emerged during illumination at wavelengths that are longer or shorter than $\lambda_{initial}$, respectively. When no feature is detected, a value of ΔA = 0 is shown.

I-rich and Br-rich phases (see Figure S26, Supporting Information) show comparable shape of the photo-miscibility-gap as the data in Figure 4. In addition, we tracked the kinetics for the change in the absorbance obtained during photo de-mixing and fitted bi-exponential functions to the data (Figures S29 and S30, Supporting Information). From the analysis of the temperature-dependent half-time we obtain an activation energy of 0.39 eV (Figure S31, Supporting Information). This value is slightly larger than the value reported for photo de-mixing in 3D (0.27 and 0.30 eV)[13,40] and 2D RP case (0.22 eV)[31] mixed halide perovskites.

In order to check the sensitivity of the boundaries of the extracted photo-miscibility-gap to the initial composition of the 2D perovskite thin film, we have performed temperature-dependent photo de-mixing on films with $x_{initial}$ = 0.4 and 0.6 (see **Figure 5**a, S32, Supporting Information), analogously to the experiment shown in Figure 4. We observe that the composition associated to the I-rich phase forming after photo de-mixing is rather insensitive to the value of $x_{initial}$. In contrast, the composition datasets extracted for the Br-rich phase seem to vary significantly depending on the pristine film composition. While the error associated with such estimates is relatively large for some of the data (see more details in Section S8, Supporting Information), this may suggest slight variations in the steady-state photo de-mixed compositions depending on the starting condition.

Based on this observation, we further test the accuracy of the methods described above, by investigating the phase stability of samples with $x_{initial}$ spanning the full range between 0 and 1. We consider the photo de-mixing of samples at 100 °C after 2 h under 1.5 mW cm^{-2} illumination intensity. Figure 5b illustrates the changes in absorbance associated to the bleach of the main excitonic peak (at the peak wavelength of the pristine film, $\lambda = \lambda_{initial}$) as well as the peaks in ΔA of features emerging due to red-shift or blue-shift of the absorption spectrum. The data reveal that changes in absorbance, and therefore possible phase instability, under light, occur for films with $x_{initial} \geq 0.15$ (see also Figures S34–S37, Supporting Information). However, the emergence of a clear Br-rich phase is only observed for $x_{initial} > 0.3$, which is consistent with our previous analysis at this temperature (see Figures 4e and 5a). Furthermore, for samples with $x_{initial} \geq 0.8$, no feature associated to an I-rich phase compared to the initial composition was detected, suggesting that no de-mixing occurred in such cases. This boundary falls within the uncertainty region of the data in Figure 5a. We note that a slight blue-shift in absorption still occurs for $x_{initial} \geq 0.8$ and even for $x_{initial} = 1$, which deserve future investigation

Importantly, we verified the "bending" of the miscibility gap observed in Figures 4 and 5a for the temperature dependence of x_I, by monitoring the kinetics of photo de-mixing in a 2D perovskite thin film with $x_{initial}$ = 0.15. When gradually decreasing the temperature from 130 to 80 °C, we observe more pronounced changes in absorbance and the clear emergence of features for both I-rich and Br-rich phases only for measurements at 80 °C (Figure S38, Supporting Information).

While the methods described above have the potential to map the miscibility gap of samples under a given illumination intensity, we acknowledge that the situation is more complicated compared to a study of a system in the dark at equilibrium. De-mixing is likely to depend on the concentration of photogenerated electronic charge carriers, and this may vary during the experiment, for example, due to changes in recombination. To test the sensitivity of the measured photo-miscibility-gap to the bias light, we ran a similar experiment as the one shown in Figure 4 with 10-times higher light intensity. We observe slight differences in the shape of the temperature-dependent absorbance of the thin film under the two light conditions, with a more pronounced excitonic signature associated to the I-rich domain at low temperatures. However, the analysis (Section S9 and Figures S39 and S40, Supporting Information) using the method described above results in surprisingly similar de-mixed compositions for the two different light intensities, suggesting limited variation in the stable compositions while varying the optical perturbation in this range.

Finally, we investigated the effect of encapsulation of the sample on the photo de-mixing behavior of these 2D perovskite thin films (Section S10 and Figure S41, Supporting Information). Similar to the previous reports on 3D perovskite films,[41] encapsulation was found to be essential to suppress the degradation of the I-rich phase, improving the reversibility of photo de-mixing and dark re-mixing. Interestingly, the non-encapsulated sample demonstrated a widening of the photo-miscibility gap when compared to a reference sample encapsulated with PMMA (data in Figure 4). Changes in absorbance for the non-encapsulated sample highlight a drop in the signature associated to I-rich domains, suggesting the presence of a loss mechanism for such phase, likely due to excorporation of iodine-based species. These observations highlight that further understanding of the role of nonstoichiometry on the thermodynamics of photo de-mixing remains a key question and point to the importance of encapsulation in the analysis of the behavior of halide perovskite materials.

Based on our analysis, we have shown the tunability of the optical properties of the 2D Dion–Jacobson perovskite films through halide substitution. Furthermore, our results on photo de-mixing of these compounds demonstrate that light-induced ion transport effects play an important role in confined 2D Dion-Jacobson systems, similarly to the case of 3D mixed-halide perovskites and 2D Ruddlesen–Popper. The complete reversibility of the process, as highlighted by our optical and structural data also indicates that no miscibility gap is present in the dark for these systems and that a thermodynamic rather than kinetic origin underlies the process of photo de-mixing in 2D films, similarly to their 3D counterparts.[42] Our study of the photo-miscibility-gap establishes the phase thermodynamics of 2D mixed-halide perovskites out-of-equilibrium experimentally. The origin of the phase instability under light may be related to selective self-trapping as suggested for 3D halide perovskites,[22,43] in addition to energetic considerations on the variation in valence band for different composition.[18] According to such model, the energies related to defect interaction with electronic charge carriers, and specifically the difference in hole trapping behavior for iodide and bromide-rich phases, would contribute to the driving force for de-mixing. However, unlike 3D systems, the large exciton binding energy in 2D perovskites[44] investigated here may also have influence on the charge carrier dynamics[31] and the interaction between the electronic charges and ionic defects. In addition, the peculiar

shape of the photo-miscibility-gap on the Br-rich side may be related to a more complex mechanism during de-mixing, such as ordering effects in the Br-rich phase. Such a "steep" shape of the miscibility gap has also been observed in calculations of 3D mixed iodide and bromide systems of $CsPbI_{1-x}Br_x$ for the I-rich phase at $x = 1/3$.[45]

3. Conclusion

In summary, we demonstrated that 2D Dion-Jacobson mixed-halide perovskites undergo photo de-mixing with conversion from the pristine $(PDMA)Pb(I_{0.5}Br_{0.5})_4$ to I-rich and Br-rich phases under illumination. In the dark, the photo de-mixed phases re-mix with complete reversibility of both their optical and structural properties, indicating full miscibility in the dark. The temperature-dependence of the photo de-mixed phases evidenced a photo-miscibility-gap in a temperature range relevant to applications of these materials in optoelectronic devices. This work thereby provides a practical approach with multiple methods for defining the thermodynamically stable compositions of hybrid perovskite mixtures under light, presenting the basis for developing a fundamental understanding of photo de-mixing in 2D mixed-halide perovskites. These findings will aid compositional engineering related to halide mixtures to enable optimization of optoelectronic devices as well as the development of other emerging systems exploiting opto-ionic effects.

4. Experimental Section

Materials: Lead iodide (PbI_2, 99.9985%) and lead bromide ($PbBr_2$, 99.999%) were purchased from Alfa Aesar. 1,4-phenylenedimethanammonium iodide ($(PDMA)I_2$) spacer, 1,4-phenylenedimethanammonium bromide ($(PDMA)Br_2$) spacer were synthesized following the procedure reported for the $(PDMA)I_2$ spacer[46] and the one described below. Dimethylsulfoxide (DMSO, 99.9%), Dimethylformamide (DMF, 99.8%), and Poly(methyl methacrylate (PMMA, average $M_w \approx 120\,000$) were purchased from Sigma-Aldrich.

Synthesis of $(PDMA)Pb(I_{1-x}Br_x)_4$ Precursor Solutions: The precursor solutions with Br content of 0%, 10%, 15%, 20%, 30%, 40%, 50% 60%, 70%, 80%, 90%, and 100% were prepared following the relative stoichiometry of the halides. Specifically, 0.33 M $(PDMA)PbI_4$ or $(PDMA)PbBr_4$ solutions were prepared by dissolving 0.33 mmol $(PDMA)I_2$ ($(PDMA)Br_2$) and 0.33 mmol PbI_2 ($PbBr_2$) in the solvent mixture of DMF and DMSO (3:2, (v:v), 200 µL). The precursor solutions for $x = 0.1$, 0.15, 0.2, 0.3, 0.4, 0.5 were prepared by dissolving $(PDMA)I_2$, PbI_2, and $PbBr_2$ with stoichiometry of $1:(1-2x):2x$. For $x = 0.6$, 0.7, 0.8, 0.9, $(PDMA)Br_2$, PbI_2, and $PbBr_2$ with stoichiometry of $1:(2-2x):(2x-1)$ were used. The synthesis of $(PDMA)Br_2$ is described in Section S1, Supporting Information.

Preparation of $(PDMA)Pb(I_{1-x}Br_x)_4$ films: The film preparation procedure was conducted in Ar-filled glovebox with controlled atmosphere (O_2 and $H_2O < 0.1$ ppm). The $(PDMA)Pb(I_{1-x}Br_x)_4$ films were deposited on quartz substrate by spin coating the precursor solution at 9 and 66 rps for 2 and 48 s, respectively. The films were annealed at 150 °C for 10 min. A PMMA encapsulation layer was deposited on perovskite films, unless stated otherwise, by drop-casting a PMMA solution (10 mg mL^{-1}, dissolved in chlorobenzene). The coated sample was dried at 40 °C for 2 h in the glovebox.

UV–Vis Spectroscopy Experiment under Controlled Conditions: UV–Vis experiments were conducted using a Shimadzu UV-2600 spectrometer. The setup was modified to achieve control of the sample temperature (1 °C accuracy) and atmosphere (<30 ppm O_2). A LED lamp (MCWHF$_2$, Thorlabs) coupled to an optical fiber was used for the illumination during the experiments. The light intensity was measured directly at the exit of the optical fiber using a thermal power meter (PM100 D, Thorlabs). The modulation of the bias light to allow for UV–Vis measurements is shown in Figure S1, Supporting Information. For each cycle, light was switched on for 900 s followed by a 300 s dark window, during which the UV–Vis measurements were taken.

X-Ray Diffraction (XRD): All the XRD patterns were acquired by a PANalytical diffractometer of Empyrean Series 2 (Cu Kα radiation, 40 kV, 40 mA) equipped with a parallel beam mirror and a PIXcel 3D detector. All measurements were conducted in Bragg-Brentano configuration modules with programmable divergence slits. The Anti scatter slits were used and recorded with a PIXcel 3D detector. The samples that were not encapsulated were mounted in a polycarbonate domed sample holder for protection from ambient atmosphere during the measurements.

Supporting Information

Supporting Information is available from the Wiley Online Library or from the author.

Acknowledgements

The authors are grateful to Helga Hoier for XRD measurements, Florian Kaiser, Udo Klock, and Dr. Rotraut Merkle for technical assistance. The authors also thank Dr. Christian Berger for providing useful feedback on this manuscript. D.M. is grateful to the Alexander von Humboldt Foundation for funding. U.R. acknowledges Swiss National Science Foundation Grant No. 200020-185092 and the NCCR-MUST for funding as well as computational resources from the Swiss National Computing Centre CSCS. This work was performed within the framework of the Max Planck-EPFL Center for Molecular Nano-science and Technology.

Open access funding enabled and organized by Projekt DEAL.

Conflict of Interest

The authors declare no conflict of interest.

Data Availability Statement

The data that support the findings of this study are openly available in Zenodo at https://doi.org/10.5281/zenodo.6525579, reference number 6525579.

Keywords

2D, mixed halide perovskites, phase stability, photo de-mixing, photo-miscibility-gap

Received: March 4, 2022
Revised: May 10, 2022
Published online:

[1] a) T. C. J. Yang, P. Fiala, Q. Jeangros, C. Ballif, *Joule* **2018**, *2*, 1421; b) K. A. Bush, K. Frohna, R. Prasanna, R. E. Beal, T. Leijtens, S. A. Swifter, M. D. McGehee, *ACS Energy Lett.* **2018**, *3*, 428.

[2] a) A. Tiwari, N. S. Satpute, C. M. Mehare, S. J. Dhoble, *J. Alloys Compd.* **2021**, *850*, 156827; b) B. R. Sutherland, E. H. Sargent, *Nat. Photonics* **2016**, *10*, 295; c) Z. K. Tan, R. S. Moghaddam,

M. L. Lai, P. Docampo, R. Higler, F. Deschler, M. Price, A. Sadhanala, L. M. Pazos, D. Credgington, F. Hanusch, T. Bein, H. J. Snaith, R. H. Friend, *Nat. Nanotechnol.* **2014**, *9*, 687.
[3] C. R. Kagan, D. B. Mitzi, C. D. Dimitrakopoulos, *Science* **1999**, *286*, 945.
[4] Y. Liu, H. Ye, Y. Zhang, K. Zhao, Z. Yang, Y. Yuan, H. Wu, G. Zhao, Z. Yang, J. Tang, *Matter* **2019**, *1*, 465.
[5] A. Kojima, K. Teshima, Y. Shirai, T. Miyasaka, *J. Am. Chem. Soc.* **2009**, *131*, 6050.
[6] J. Cho, J. T. DuBose, P. V. Kamat, *J. Phys. Chem. Lett.* **2020**, *11*, 2570.
[7] a) Y. Chen, Y. Sun, J. Peng, J. Tang, K. Zheng, Z. Liang, *Adv. Mater.* **2018**, *30*, 1703487; b) C. C. Stoumpos, D. H. Cao, D. J. Clark, J. Young, J. M. Rondinelli, J. I. Jang, J. T. Hupp, M. G. Kanatzidis, *Chem. Mater.* **2016**, *28*, 2852.
[8] a) L. Mao, W. Ke, L. Pedesseau, Y. Wu, C. Katan, J. Even, M. R. Wasielewski, C. C. Stoumpos, M. G. Kanatzidis, *J. Am. Chem. Soc.* **2018**, *140*, 3775; b) J. V. Milić, J.-H. Im, D. J. Kubicki, A. Ummadisingu, J.-Y. Seo, Y. Li, M. A. Ruiz-Preciado, M. I. Dar, S. M. Zakeeruddin, L. Emsley, M. Grätzel, *Adv. Energy Mater.* **2019**, *9*, 1900284.
[9] N. Mercier, *Angew. Chem., Int. Ed.* **2019**, *58*, 17912.
[10] J. H. Noh, S. H. Im, J. H. Heo, T. N. Mandal, S. I. Seok, *Nano Lett.* **2013**, *13*, 1764.
[11] M. G. La-Placa, D. Y. Guo, L. Gil-Escrig, F. Palazon, M. Sessolo, H. J. Bolink, *J. Mater. Chem. C* **2020**, *8*, 1902.
[12] I. Karimata, T. Tachikawa, *Angew. Chem., Int. Ed.* **2021**, *60*, 2548.
[13] E. T. Hoke, D. J. Slotcavage, E. R. Dohner, A. R. Bowring, H. I. Karunadasa, M. D. McGehee, *Chem. Sci.* **2015**, *6*, 613.
[14] W. Mao, C. R. Hall, A. S. R. Chesman, C. Forsyth, Y.-B. Cheng, N. W. Duffy, T. A. Smith, U. Bach, *Angew. Chem., Int. Ed.* **2019**, *58*, 2893.
[15] F. Brivio, C. Caetano, A. Walsh, *J. Phys. Chem. Lett.* **2016**, *7*, 1083.
[16] F. Lehmann, A. Franz, D. M. Többens, S. Levcenco, T. Unold, A. Taubert, S. Schorr, *RSC Adv.* **2019**, *9*, 11151.
[17] a) C. G. Bischak, A. B. Wong, E. Lin, D. T. Limmer, P. D. Yang, N. S. Ginsberg, *J. Phys. Chem. Lett.* **2018**, *9*, 3998; b) Y. Zhou, L. You, S. Wang, Z. Ku, H. Fan, D. Schmidt, A. Rusydi, L. Chang, L. Wang, P. Ren, L. Chen, G. Yuan, L. Chen, J. Wang, *Nat. Commun.* **2016**, *7*, 11193; c) T.-C. Wei, H.-P. Wang, T.-Y. Li, C.-H. Lin, Y.-H. Hsieh, Y.-H. Chu, J.-H. He, *Adv. Mater.* **2017**, *29*, 1701789; d) C. G. Bischak, C. L. Hetherington, H. Wu, S. Aloni, D. F. Ogletree, D. T. Limmer, N. S. Ginsberg, *Nano Lett.* **2017**, *17*, 1028.
[18] S. Draguta, O. Sharia, S. J. Yoon, M. C. Brennan, Y. V. Morozov, J. S. Manser, P. V. Kamat, W. F. Schneider, M. Kuno, *Nat. Commun.* **2017**, *8*, 200.
[19] A. Ruth, M. C. Brennan, S. Draguta, Y. V. Morozov, M. Zhukoyskyi, B. Janko, P. Zapol, M. Kuno, *ACS Energy Lett.* **2018**, *3*, 2321.
[20] R. A. Belisle, K. A. Bush, L. Bertoluzzi, A. Gold-Parker, M. F. Toney, M. D. McGehee, *ACS Energy Lett.* **2018**, *3*, 2694.
[21] R. A. Kerner, Z. J. Xu, B. W. Larson, B. P. Rand, *Joule* **2021**, *5*, 2273.
[22] a) G. Y. Kim, A. Senocrate, T. Y. Yang, G. Gregori, M. Gratzel, J. Maier, *Nat. Mater.* **2018**, *17*, 445; b) G. Y. Kim, A. Senocrate, Y.-R. Wang, D. Moia, J. Maier, *Angew. Chem., Int. Ed.* **2021**, *60*, 820.
[23] J. T. DuBose, P. V. Kamat, *J. Am. Chem. Soc.* **2020**, *142*, 5362.
[24] G. F. Samu, Á. Balog, F. De Angelis, D. Meggiolaro, P. V. Kamat, C. Janáky, *J. Am. Chem. Soc.* **2019**, *141*, 10812.
[25] L. A. Frolova, S. Y. Luchkin, Y. Lekina, L. G. Gutsev, S. A. Tsarev, I. S. Zhidkov, E. Z. Kurmaev, Z. X. Shen, K. J. Stevenson, S. M. Aldoshin, P. A. Troshin, *Adv. Energy Mater.* **2021**, *11*, 2002934.
[26] A. Senocrate, E. Kotomin, J. Maier, *Helv. Chim. Acta* **2020**, *103*, 8.
[27] X. Xiao, J. Dai, Y. J. Fang, J. J. Zhao, X. P. Zheng, S. Tang, P. N. Rudd, X. C. Zeng, J. S. Huang, *ACS Energy Lett.* **2018**, *3*, 684.
[28] J. Cho, J. T. DuBose, A. N. T. Le, P. V. Kamat, *ACS Mater. Lett.* **2020**, *2*, 565.
[29] A. M. Tirmzi, R. P. Dwyer, F. Y. Jiang, J. A. Marohn, *J. Phys. Chem. C* **2020**, *124*, 13639.
[30] a) P. S. Mathew, J. T. DuBose, J. Cho, P. V. Kamat, *ACS Energy Lett.* **2021**, *6*, 2499; b) Y. Liu, M. Wang, A. V. Ievlev, M. Ahmadi, B. Hu, O. S. Ovchinnikova, arXiv:2107.00786 **2021**.
[31] J. Cho, P. S. Mathew, J. T. DuBose, P. V. Kamat, *Adv. Mater.* **2021**, *33*, 2105585.
[32] A. J. Knight, J. B. Patel, H. J. Snaith, M. B. Johnston, L. M. Herz, *Adv. Energy Mater.* **2020**, *10*, 1903488.
[33] a) M. C. Gélvez-Rueda, P. Ahlawat, L. Merten, F. Jahanbakhshi, M. Mladenović, A. Hinderhofer, M. I. Dar, Y. Li, A. Dučinskas, B. Carlsen, W. Tress, A. Ummadisingu, S. M. Zakeeruddin, F. Schreiber, A. Hagfeldt, U. Rothlisberger, F. C. Grozema, J. V. Milić, M. Graetzel, *Adv. Funct. Mater.* **2020**, *30*, 2003428; b) Y. Li, J. V. Milić, A. Ummadisingu, J.-Y. Seo, J.-H. Im, H.-S. Kim, Y. Liu, M. I. Dar, S. M. Zakeeruddin, P. Wang, A. Hagfeldt, M. Grätzel, *Nano Lett.* **2019**, *19*, 150; c) A. Dučinskas, G. Y. Kim, D. Moia, A. Senocrate, Y.-R. Wang, M. A. Hope, A. Mishra, D. J. Kubicki, M. Siczek, W. Bury, T. Schneeberger, L. Emsley, J. V. Milić, J. Maier, M. Grätzel, *ACS Energy Lett.* **2021**, *6*, 337; d) A. Ummadisingu, A. Mishra, D. J. Kubicki, T. LaGrange, A. Dučinskas, M. Siczek, W. Bury, J. V. Milić, M. Grätzel, L. Emsley, *Small* **2022**, *18*, 2104287.
[34] M. Baranowski, P. Plochocka, *Adv. Energy Mater.* **2020**, *10*, 1903659.
[35] G. Lanty, K. Jemli, Y. Wei, J. Leymarie, J. Even, J. S. Lauret, E. Deleporte, *J. Phys. Chem. Lett.* **2014**, *5*, 3958.
[36] F. Babbe, C. M. Sutter-Fella, *Adv. Energy Mater.* **2020**, *10*, 1903587.
[37] a) S. J. Yoon, M. Kuno, P. V. Kamat, *ACS Energy Lett.* **2017**, *2*, 1507; b) W. X. Huang, S. J. Yoon, P. Sapkota, *ACS Appl. Energy Mater.* **2018**, *1*, 2859.
[38] P. S. Mathew, J. T. DuBose, J. Cho, P. V. Kamat, *ACS Energy Lett.* **2021**, *6*, 2499.
[39] Y.-R. Wang, G. Y. Kim, E. Kotomin, D. Moia, J. Maier, *J. Phys.: Energy* **2022**, *4*, 011001.
[40] T. Elmelund, B. Seger, M. Kuno, P. V. Kamat, *ACS Energy Lett.* **2020**, *5*, 56.
[41] A. J. Knight, A. D. Wright, J. B. Patel, D. P. McMeekin, H. J. Snaith, M. B. Johnston, L. M. Herz, *ACS Energy Lett.* **2019**, *4*, 75.
[42] G. C. Halford, Q. Deng, A. Gomez, T. Green, J. M. Mankoff, R. A. Belisle, *ACS Appl. Mater. Interfaces* **2022**, *14*, 4335.
[43] a) R. A. Evarestov, E. A. Kotomin, A. Senocrate, R. K. Kremer, J. Maier, *Phys. Chem. Chem. Phys.* **2020**, *22*, 3914; b) R. A. Evarestov, A. Senocrate, E. A. Kotomin, J. Maier, *Phys. Chem. Chem. Phys.* **2019**, *21*, 7841.
[44] O. Yaffe, A. Chernikov, Z. M. Norman, Y. Zhong, A. Velauthapillai, A. van der Zande, J. S. Owen, T. F. Heinz, *Phys. Rev. B* **2015**, *92*, 045414.
[45] a) J. S. Bechtel, A. Van der Ven, *Phys. Rev. Mater.* **2018**, *2*, 7; b) W.-J. Yin, Y. Yan, S.-H. Wei, *J. Phys. Chem. Lett.* **2014**, *5*, 3625.
[46] Y. Li, J. V. Milic, A. Ummadisingu, J. Y. Seo, J. H. Im, H. S. Kim, Y. Liu, M. I. Dar, S. M. Zakeeruddin, P. Wang, A. Hagfeldt, M. Gratzel, *Nano Lett.* **2019**, *19*, 150.